Wide-Area Measurement Based Dynamic Stochastic Optimal Power Flow Control for Smart Grids With High Variability and Uncertainty

Jiaqi Liang, *Student Member, IEEE*, Ganesh K. Venayagamoorthy, *Senior Member, IEEE*, and Ronald G. Harley, *Fellow, IEEE*

***Abstract*—To achieve a high penetration level of intermittent renewable energy, the operation and control of power systems need to account for the associated high variability and uncertainty. Power system stability and security need to be ensured dynamically as the system operating condition continuously changes. A wide-area measurement based dynamic stochastic optimal power flow (DSOPF) control algorithm using the adaptive critic designs (ACDs) is presented in this paper. The proposed DSOPF control replaces the traditional AGC and secondary voltage control, and provides a coordinated AC power flow control solution to the smart grid operation in an environment with high short-term uncertainty and variability. The ACD technique, specifically the dual heuristic dynamic programming (DHP), is used to provide nonlinear optimal control, where the control objective is explicitly formulated to incorporate power system economy, stability and security considerations. The proposed DSOPF controller dynamically drives the power system to its optimal operating point by continuously adjusting the steady-state set points sent by the traditional OPF algorithm. A 12-bus test power system is used to demonstrate the development and effectiveness of the proposed DSOPF controller.**

***Index Terms*—Adaptive critic designs, dynamic stochastic optimal power flow control, intelligent control, smart grid, wide-area control.**

I. Introduction

WITH THE increasing penetration of intermittent renewable energy, power systems encounter more and more uncertainty and variability. How to reliably and efficiently operate a power system in such an environment is still an unanswered challenging question [1], [2]. With the state-of-the-art wind forecasting methods, the hour-ahead forecast errors for a single wind plant are still around 10%–15% with respect to its actual outputs [3]. With much lower forecasting errors for load, the traditional power system operation is based on deterministic security-constrained commitment and dispatch processes [4], which tend to be conservative (using forecasts with a high probability of exceedance) when intermittent renewable generation is considered [2]. This conservative operation contributes somewhat to a large amount of wind curtailment [5], as secure operation cannot be guaranteed in real time when the actual wind power significantly exceeds the forecasts used in the scheduling and dispatching processes.

The optimal power flow (OPF), or its security-constrained version, is based on steady-state optimization without considering local controller and load dynamics, and its optimal solutions are obtained based on forecasts. With uncertainty from renewable generation and storage, the convexity of the OPF problem has been studied recently [6], [7]. Although the OPF provides optimal dispatches for the next forecasted period, any unforeseen real-time load/generation variation or postcontingency operation between two dispatch instants (typically 5 min apart) are handled by simple linear controllers or some predefined reactions with little, if any, system-wide optimization. For real-time active power balancing, the proportional-integral-controller-based automatic generation control (AGC) is typically used [8]. For reactive power support, locally-controlled reactive resources are typically used for voltage regulation, such as large generators equipped with automatic voltage regulators (AVRs), switched capacitor banks, on-load tap changing (OLTC) transformers, and flexible ac transmission system (FACTS) devices [8].

The development of wide-area measurement systems (WAMSs), based on synchronized phasor measurement units (PMUs) [9], greatly improves the power grid observability, even during transient events [10]. WAMSs enable distributed dynamic state estimation, which can dramatically reduce the reporting time of the global system states (from minutes down to fractions of a second) and improve the grid visibility from steady states to dynamics [11], [12]. With the global dynamic information, advanced wide-area control (WAC) schemes become possible to improve grid dynamics. Most of the WAC schemes to date have focused on power system stability related issues, including the transient/small-signal stabilizing control to mitigate angle instability [13]–[21], and the secondary voltage control to mitigate voltage instability [22]–[25]. The design of a system-wide automatic power flow controller to dynamically control a power system to its optimal operating point has received little attention.

Fardanesh [26] described an ideal control scenario for power systems, where the optimal operating condition was achieved continuously by some closed-loop control algorithms, but how

Manuscript received January 17, 2011; revised June 02, 2011, August 04, 2011; accepted October 14, 2011. This work was supported in part by the U.S. National Science Foundation, under Grants ECCS 0348221, ECCS GOALI 0802047 and EFRI 0836017. Any opinions, findings, and conclusions or recommendations expressed in this work are those of the authors and do not necessarily reflect the views of the National Science Foundation. Paper no. TSG-00006-2011.

J. Liang is with the School of Electrical and Computer Engineering, Georgia Institute of Technology, Atlanta, GA 30332 USA. (e-mail: jliang@gatech.edu).

G. K. Venayagamoorthy is with the Holcombe Department of Electrical and Computer Engineering, Clemson University, Clemson, SC 29634 USA (e-mail: gkumar@ieee.org).

R. G. Harley is with the School of Electrical and Computer Engineering, Georgia Institute of Technology, Atlanta, GA 30332 USA and also Professor Emeritus and Honorary Research Associate with the University of KwaZulu-Natal, Durban, South Africa. (e-mail: rharley@gatech.edu).

Color versions of one or more of the figures in this paper are available online at http://ieeexplore.ieee.org.

Digital Object Identifier 10.1109/TSG.2011.2174068

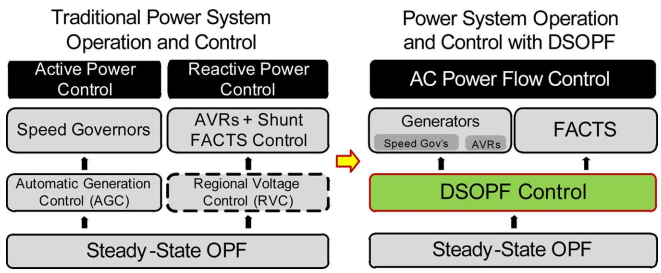

Fig. 1. Traditional operation-control structure of a power system and the proposed structure with DSOPF control.

to design such a control algorithm remained unanswered. A conceptual framework of applying the adaptive critic designs (ACDs) [27]–[29] to power system optimizations, namely dynamic stochastic optimizations, was first proposed by Venayagamoorthy [30] and then by Momoh [31] to incorporate prediction and optimization over power system stochastic disturbances. However, detailed designs and analyses have not been reported.

This paper details the dynamic stochastic optimization concept, and presents a wide-area measurement based dynamic stochastic optimal power flow (DSOPF) control scheme for smart grids. A power system is a multi-input multi-output (MIMO), nonlinear, and nonstationary complex dynamic plant. An ACD-based intelligent controller is designed to replace the traditional AGC and secondary/regional voltage control, as illustrated in Fig. 1, and provide nonlinear optimal control to the system-wide ac power flow. An optimal control objective is explicitly defined in the ACD technique. Thus, the operating cost and different stability and security indices of interest can be readily formulated in the control objective.

An overview of the existing power system WAC schemes is provided in Section II. Section III introduces the DSOPF control concept and discusses its implementation using ACDs. A 12-bus test power system is used as an example in Section IV to design a DSOPF controller using the dual heuristic dynamic programming (DHP), a technique in the ACD family. Simulation results and case studies are provided in Section V to demonstrate the effectiveness of the DSOPF controller.

II. Overview of Wide-Area Control in Power Systems

Power system WAC in general includes any control algorithms that require monitoring signals or control actions to be transmitted over a large geographic area [10].

A. Transient/Small-Signal Stabilizing Control

Local damping controllers are usually ineffective in damping interarea oscillations [13], which are characterized by groups of coherent generators swinging against each other. Because of the complexity, nonlinearity, and time-varying characteristics of a power system, designing a wide-area stabilizing controller over a wide operation range is not a trivial task. Kamwa *et al.* [13] decoupled the MIMO power system into several single-input single-output (SISO) global stabilizing loops based on coupling between different input-output pairs. The SISO global loops were then sequentially optimized. Instead of multiple SISO loops, the observer-based state feedback (SF) linear control [15] and the robust H∞ control using linear matrix inequality (LMI) [19] were applied to design a MIMO damping controller. Because of the linear nature of both the SF and H∞-LMI control designs, different control loops were thus designed at different operating points and switched by a probabilistic-model-reference method in [15] and a fuzzy-inference system in [19]. Others approached the problem directly from the nonlinear analytical model of power systems [20], [21], where the resulting controller parameters depend on system operating conditions and need to be continuously estimated.

The above control techniques all suffer from requiring detailed knowledge of system model and parameters, which are usually difficult to obtain for complex power systems. More advanced computational-intelligence-based controllers using the ACD technique have been reported [16]–[18] and showed a promising performance compared to the observer-based SF and H∞-LMI controllers [17]. ACDs require no analytical model and enable controllers to deal with nonlinear nonstationary systems in the presence of noise and uncertainty [29].

B. Secondary Frequency and Voltage Control

The earliest example of closed-loop wide-area control is perhaps the AGC [32], which is also known as secondary frequency control. AGC uses a simple PI controller to regulate the system frequency and interarea power flow and maintain the real-time generation-demand balance in its control area [8]. Generation adjustment commands for individual generators are coordinated by predefined ratios or ratios from economic dispatch [8]. The reinforcement learning technique has recently been applied to improve the robustness and dynamic performances of the traditional AGC design [33]. In North America, AGC commands are typically updated every 2–4 s [8]. Although AGC provides system-wide active power control, it treats the grid as a single bus, has no coordination with the system reactive power control, and does not consider system stability and security.

Automatic secondary/regional voltage control is under development in some countries, such as Italy, where the power system has been divided into separate voltage regulation regions with each region having its own pilot node (bus) [22], [23]. The main generators in each region are used to regulate the pilot node voltage with a PI regulator [22], where commands are updated at an interval not exceeding 2 s [23]. Wang *et al.* [24] proposed a finite-state machine coordinated fuzzy controller to control multiple shunt FACTS devices and maintain system-wide voltages. Nonlinear model predictive control (NMPC) has also been reported to control system-wide voltages by optimally selecting control commands from a pool of possible control actions [25].

The present separate secondary control loops for frequency and voltage are developed based on the assumption that only small variations and uncertainty exist in power systems during a short period of time, and long-term large variations are handled by sequential steady-state optimizations (e.g., OPF). This assumption is true when the only uncertain factor in a power system is the load, which varies relatively slow at the transmission level and is well predictable because of its cycling characteristics. However, in an environment with high variability and uncertainty, significant power flow redistribution may occur in a short period. A better or more sophisticated real-time correction/control method would be required to ensure system security. With the present frequency and voltage control schemes, power line overloading and bus over/under-voltage may occur due to the limited control capability of AGC and limited local reactive power resources. A system-wide active and reactive power

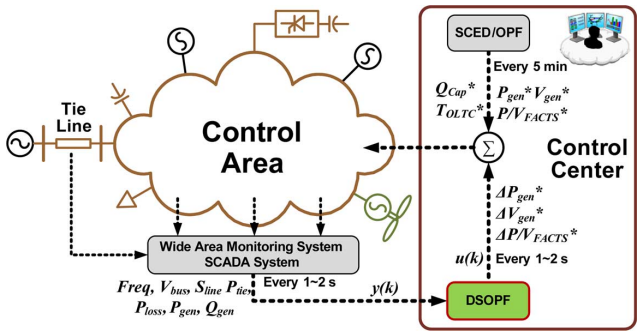

Fig. 2. General framework of DSOPF control ($P_{\rm gen}$ and $V_{\rm gen}$ are commands to generator units; $P/V_{\rm FACTS}$ are commands to FACTS devices; $Q_{\rm Cap}$ are commands to switched capacitor banks; $T_{\rm OLTC}$ are commands to OLTC transformers).

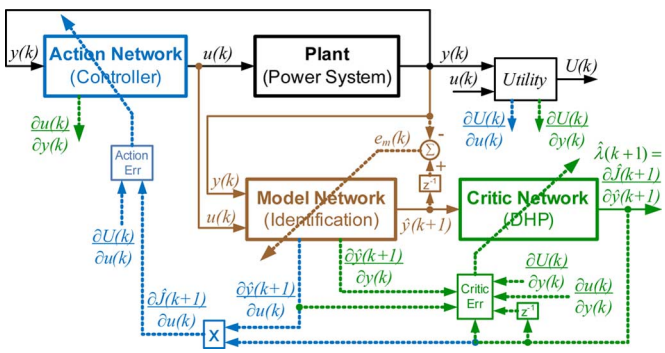

Fig. 3. Schematic diagram of neurocontrol design using DHP. Color codes: Brown denotes signals for training model network, green denotes signals for training critic network, and blue denotes signals for training action network.

coordinated control algorithm is thus necessary in a high-variability environment.

III. Dynamic Stochastic Optimal Power Flow Control

A. Framework of the Proposed DSOPF Control

The power system is assumed to be sufficiently observable with WAMSs. Data preprocessing/concentrating/transmitting in WAMSs, state estimations, and derivations of other power system quantities are not considered in this paper. Continuous snapshots of the dynamic power system are assumed to be readily available in the control room.

With continuous snapshots as system feedbacks, the job of a DSOPF controller is to dynamically adjust the steady-state commands generated by the OPF algorithm, as shown in Fig. 2. To obtain an optimal real-time dynamic dispatch, both the real and reactive power flows are controlled simultaneously. Under a high short-term variability environment, only those continuously adjustable resources are controlled by the DSOPF controller to continuously track the optimal operating point, leaving the lifetime of the mechanical-switch-based devices unaffected.

A nonlinear optimal control strategy is necessary to achieve the DSOPF control, where an objective function (the cost-to-go function) is minimized in a closed-loop control fashion and the nonlinearity is used to handle different operating points and physical control limits. Besides the optimality and nonlinearity considerations, the DSOPF control must be able to adapt to the time-varying dynamics of a power system, whose topology may change at any point in time. To implement the DSOPF, it is thus essential to have a nonlinear optimal control strategy that is able to continuously identify the system topology changes and adjust its optimal control laws accordingly. The ACD technique is thus a promising candidate for designing the DSOPF controller.

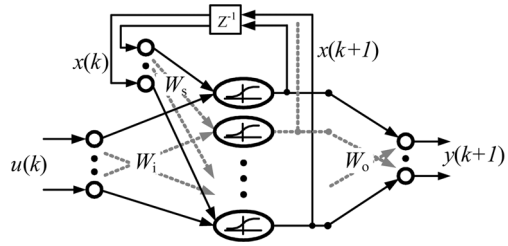

Fig. 4. Structure of a hidden-layer-feedback RNN.

B. Adaptive Critic Designs (ACDs) for Implementing DSOPF

A family of ACDs was proposed by Werbos as a new optimal control technique combining the concepts of reinforcement learning and approximate dynamic programming [27]. This technique has been applied in areas including robotic control, missile control, flight control, etc. [29]. A nonlinear optimal controller for a STATCOM [34] and a nonlinear optimal wide-area damping controller for a 12-bus system [18] have also been successfully designed using ACDs. Venayagamoorthy *et al.* [35] has reported successful hardware implementation of an ACD-based optimal damping controller for turbogenerators in a multimachine system.

The ACD technique uses a neural network, namely the critic network, to approximate the cost-to-go function J in Bellman's equation of dynamic programming, in a step-by-step manner as follows:

$$J(k) = \sum_{i=0}^{\infty} \gamma^i \cdot U(k+i), \tag{1}$$

where γ $(0 < \gamma < 1)$ is a discount factor, and $U(k)$ is the utility function (a present cost to be minimized at time k). The optimal control problem is to generate control action $u(k)$ that minimizes $J(k)$ at each time step k. For the DSOPF control, $U(k)$ could be a function of the total energy cost, bus voltage deviations, frequency deviation, tie-line flow deviations, line loadings, line losses, generator stability margins, and/or other indices related to the system economy, stability, and security.

The schematic diagram of the DHP algorithm [29] is shown in Fig. 3, where the *critic* network directly estimates the gradient of $J(k)$. A *model* neural network is used to continuously identify the plant (power system) dynamics and provide a nonlinear differentiable plant model. An *action* neural network is trained to minimize (1) and to approximate the optimal control laws. $y(k)$ denotes the plant output at time k, and $u(k)$ denotes the controller action. The various partial derivative signals are used for training the three neural networks. More details on the mathematical background of ACDs and training algorithms for DHP can be found in [29].

C. Recurrent Neural Networks for ACDs

Recurrent neural networks (RNNs), as shown in Fig. 4, are used to implement the model network, critic network and action network in this paper. RNNs have advantages over other static feed-forward neural networks (FFNNs) in modeling and control of dynamic systems due to their internal dynamic memories [36]. A power system identifier for eigenvalue extraction has been designed using a specific type of RNNs [37]. Different

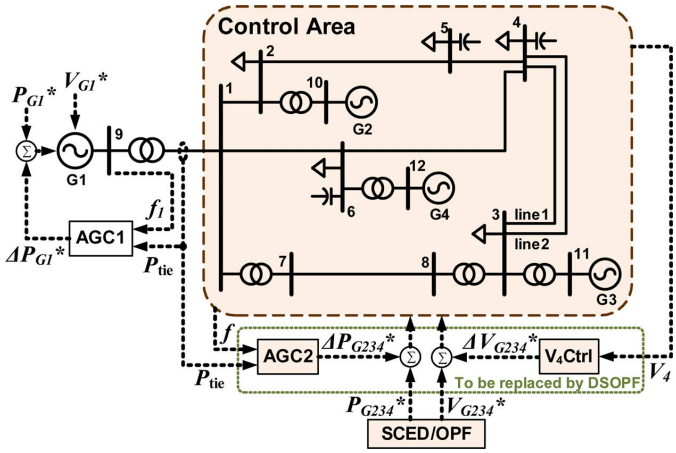

Fig. 5. 12-bus test power system with AGCs and voltage control on pilot bus 4.

training algorithms for RNNs have been discussed [36], [38], [39], and will not be repeated in this paper.

For neurocontrol designs using FFNNs, time delayed loops (TDLs), which provide the neural network with a series of previous plant input-output signals, are necessary to model the plant dynamics [40]. With RNNs, their internal dynamic loops effectively provide the time delayed information [41], and thus TDLs are not used in the schematic diagram shown in Fig. 3. More mathematical background on using RNNs for implementing DHP has been discussed by the authors in [41].

IV. DHP-Based DSOPF Controller Design for a 12 Bus Test Power System

A. Bus Test Power System

A 12-bus test power system modified from [42], as shown in Fig. 5, is used to demonstrate the design of a DHP-based DSOPF controller. Buses 4 and 5 are two remote load buses supplied from three transmission corridors. No infinite bus is used to hold the system frequency. All four generators are modeled with full transient dynamics in PSCAD and equipped with AVRs and speed governors. Generators 2 to 4 are within one control area and they are controlled by AGC2. Generator 1 is assumed to be an aggregated representation of an interconnected area and it is controlled by AGC1. With AGC1 and AGC2, the system frequency and interarea tie-line power flow, $P_{\rm tie}$, can be maintained at the nominal/scheduled values. Bus 4 is selected as the pilot bus for a PI-based secondary voltage control. Block diagrams of the AGC, bus 4 voltage control ($\rm V_4Ctrl$), AVR, and speed governor used in this paper are shown in Fig. 6. The dispatch ratios in the AGC, K_{G1}, K_{G2}, and K_{G3}, are determined by the changing rate of the incremental cost of each generator, so that any changes from the AGC would result in minimum costs [8]. The dispatch ratios in the $\rm V_4Ctrl$ are set to be equal in this study. All four generators are assumed to be gas-turbine based and have a ramp rate (both up and down) of 18 MW/min.

The generator and line parameters are provided in [42]. The base case of this system, including the scheduled tie-line flow, is defined in the Appendix. At each load bus, half of the load is represented by a constant-power load and the other half is represented by a constant-impedance load, which introduces some

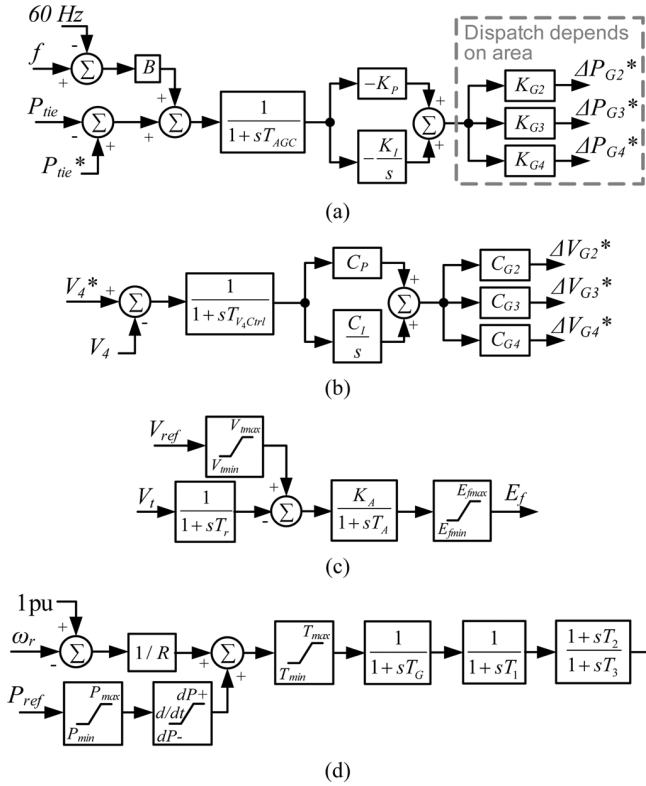

Fig. 6. Block diagrams of: (a) an PI-based AGC ($P_{\rm tie}$ is positive with an inbound flow); (b) a PI-based pilot bus voltage control; (c) an AVR; and (d) a speed governor.

load-voltage characteristics [43]. All lines are represented by the lumped π-equivalent model [8].

A DSOPF controller is designed below to replace AGC2 and $\rm V_4Ctrl$ and provide coordinated secondary active and reactive power flow control. AGC2 and $\rm V_4Ctrl$ are disconnected during the training and testing of the DSOPF controller. Similar to AGC, the data update rate for the DSOPF controller is assumed to be 1 s, which neglects the transient oscillations but includes the local controller and load dynamics. During the training, the weights of the model, action, and critic networks in the ACD scheme are also updated every 1 s.

B. Model Network—System Identification

The nonlinear dynamic plant seen by the DSOPF controller is defined in Fig. 7. The following 15 smoothed wide-area measurements are sampled at 1 Hz for the DSOPF controller: the system frequency in Hz, f (average rotor speeds of G2, G3 and G4); the rms voltage at each of the 5 load buses in per unit (pu), V_2, V_3, V_4, V_5, and V_6; the apparent power flow magnitude of 4 long lines in pu, S_{25}, S_{16}, S_{64}, and S_{78}; the tie-line power import in MW, $P_{\rm tie}$; the active power outputs from G2 to G4 in MW, P_{G2}, P_{G3}, and P_{G4}; and the total active power loss in MW, $P_{\rm loss}$. These 15 measurements are then scaled linearly to have the same order of magnitude, and the plant output, $y(k)$, is obtained.

The plant has 6 inputs from the DSOPF controller. $u_1(k)$ to $u_3(k)$ are adjustment signals to change the three generators' active power outputs, and $u_4(k)$ to $u_6(k)$ are adjustment signals to change the three generators' terminal voltages. These six inputs are scaled and added to the steady-state dispatches, u^*, obtained from the traditional OPF algorithm.

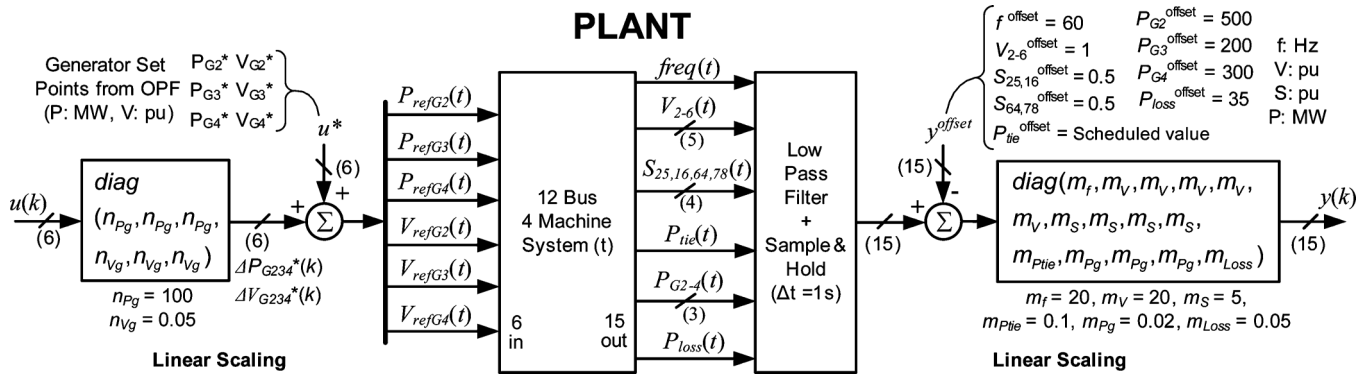

Fig. 7. The nonlinear plant seen by the DHP-based DSOPF controller in the 12-bus power system example.

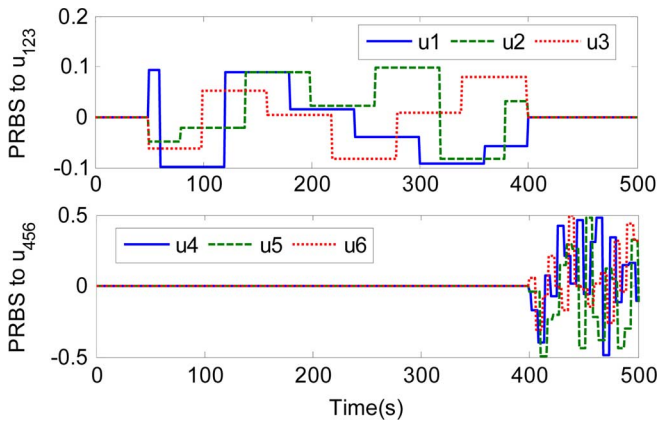

Fig. 8. PRBS perturbations applied to the 12-bus system.

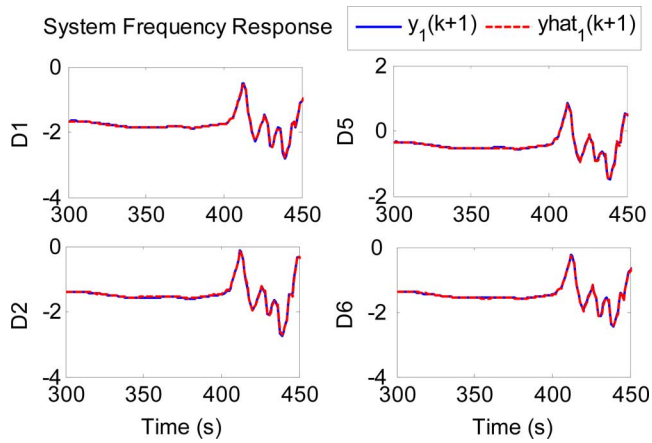

Fig. 9. Model network testing results at the D1, D2, D5, and D6: plant output $y_1(k+1)$ and model network output $\hat{y}_1(k+1)$.

Based on the DHP scheme shown in Fig. 3, an RNN model network, with 21 inputs and 15 outputs, is trained to minimize the following error [29]:

$$E_m(k) = \|e_m(k)\|^2 = \|y(k) - \hat{y}(k)\|^2 \tag{2}$$

where $\hat{y}(k)$ is obtained from one step delay of the model network output. In other words, the model network is trained to identify the plant dynamics and provide one-step-ahead prediction. The model network is pretrained with pseudo-random binary signal (PRBS) injections at 8 different dispatch cases, as listed in Table I, where D1 is the base case, D2–D4 represent line outage conditions, and D5–D8 represent different load conditions. All 8 dispatches have been optimized in MATPOWER [44] using the interior-point OPF algorithm with bus-voltage and line-rating constraints, and then manually adjusted to account for load-voltage characteristics and local controller errors. The PRBS perturbations applied to the system are shown in Fig. 8, where the perturbations applied to the 3 generator power commands change sequentially every 20 s, and the perturbations applied to the three generator voltage commands change sequentially every 2 s. 500 s of data for each dispatch case are recorded and used for model pretraining.

The testing results of the pretrained model network (with fixed weights) at D1, D2, D5, and D6 under the same PRBS injections are shown in Fig. 9, where only y_1 (related to the system frequency) is plotted due to limited space. All 15 outputs from the model network have similar tracking performances at all 8 dispatch cases. After the pretraining, the model network is then used to provide the system-wide cross-coupling sensitivity signals, $\partial y(k+1)/\partial u(k)$, over a wide operation range for training the critic and action networks. During the training of critic and action networks, the model weights are continuously updated with a small learning rate to ensure tracking of new operating conditions.

TABLE I
OPERATING CONDITIONS FOR MODEL NETWORK PRETRAINING

Dispatch	G2		G3		G4		Line or load changes from base case (P: MW, Q: MVAr)
	P_{G2}* (MW)	V_{G2}* (pu)	P_{G3}* (MW)	V_{G3}* (pu)	P_{G4}* (MW)	V_{G4}* (pu)	
D1	500	1.02	200	1.01	300	1.02	None (Base Case)
D2	490	1.02	220	1.03	330	1.03	Line 2-5 is out
D3	500	1.03	215	1.04	300	1.02	Line 4-6 is out
D4	500	1.03	215	1.04	315	1.04	One of lines 3-4 is out
D5	550	1.05	270	1.04	360	1.02	Const. power load at buses 3&5 become: P_{L3} =210, Q_{L3} = 140 P_{L5} =100, Q_{L5} = 50
D6	505	0.99	180	1.02	285	1.03	Const. power load at bus 5 becomes: P_{L5} = 0, Q_{L5} = 0
D7	525	1.02	250	1.04	340	1.03	Const. power load at bus 4 becomes: P_{L4} = 210, Q_{L4} = 140
D8	500	1.01	190	1.02	290	1.02	Const. power load at bus 4 becomes: P_{L4} = 110, Q_{L4} = 100

P_{G1}*, V_{G1}*, and P_{tie}* are the same as the base case for all dispatch cases.

C. Critic Network and Cost-to-Go Function—Optimal Control Objective

The control objective for the 12-bus system in this paper includes six components: the area control error, $U_{\rm ACE}$; the system voltage deviation, $U_{\rm Volt}$; the system line loading, $U_{\rm Line}$; the total fuel cost, $U_{\rm Fuel}$; the total line loss, $U_{\rm Loss}$; and the control effort, $U_{\rm Ctrl}$. The utility function, U, is thus defined as

$$U(k) = U_{\rm ACE}(k) + U_{\rm Volt}(k) + U_{\rm Line}(k) + U_{\rm Fuel}(k) + U_{\rm Loss}(k) + U_{\rm Ctrl}(k), \quad (3)$$

with

$$\begin{aligned} U_{\rm ACE}(k) &= w_{\rm freq}\Delta f^2(k) + w_{\rm tie}\Delta P_{\rm tie}^2(k) \\ &= w_{\rm freq} y_1^2(k)/m_f^2 + w_{\rm tie} y_{11}^2(k)/m_{P\rm tie}^2 \\ U_{\rm Volt}(k) &= w_{\rm volt}\|\Delta V_{2-6}(k)\|^2 \\ &= w_{\rm volt}\|y_{2-6}(k)\|^2/m_V^2 \\ U_{\rm Line}(k) &= w_{\rm line}\Big[e^{(S_{25}^4(k)-1)} + e^{(S_{16}^4(k)-1)} \\ &\quad + e^{(S_{64}^4(k)-1)} + e^{(S_{78}^4(k)-1)}\Big] \\ U_{\rm Fuel}(k) &= w_{\rm fuel}[F_{G2}(k) + F_{G3}(k) \\ &\quad + F_{G4}(k) - F^{\rm offset}] \\ U_{\rm Loss}(k) &= w_{\rm loss}P_{\rm loss}(k) \\ &= w_{\rm loss}\left[y_{15}(k)/m_{\rm Loss} + P_{\rm loss}^{\rm offset}\right] \\ U_{\rm Ctrl}(k) &= w_{Pg}\|\Delta P_{G2-4}^*(k)\|^2 + w_{Vg}\|\Delta V_{G2-4}^*(k)\|^2 \\ &= w_{Pg}n_{\rm Pg}^2\|u_{1-3}(k)\|^2 + w_{Vg}n_{Vg}^2\|u_{4-6}(k)\|^2, \end{aligned} \quad (4)$$

where w_x's are various weighting factors (listed in the Appendix), and m_x's and n_x's are the plant input-output scaling factors shown in Fig. 7. In this paper, the weighting factors are heuristically selected. A higher weighting factor gives a higher priority to the corresponding component, and these weights may be changed according to system conditions and specific designs. $U_{\rm Line}$(k) in (4) is designed such that if a line loading is above 1 pu, $U_{\rm Line}$(k) increases dramatically; otherwise, $U_{\rm Line}$(k) becomes negligible. The pu line loading of line 2–5, $S_{25}(k)$, is obtained by

$$S_{25}(k) = \left[y_7(k)/m_s + S_{25}^{\rm offset}\right]. \quad (5)$$

Similar relationships exist between $S_{16}(k)$, $S_{64}(k)$, $S_{78}(k)$ and $y_8(k)$, $y_9(k)$, $y_{10}(k)$, respectively. In (4), $F_{\rm Gi}$(k) is the fuel cost of generator i in \$/h. A quadratic function is used to approximate the generator fuel cost, as in

$$\begin{aligned} F_{Gi}(k) &= a_i + b_i P_{Gi}(k) + c_i P_{Gi}^2(k) \\ P_{Gi}(k) &= y_{10+i}(k)/m_{Pg} + P_{Gi}^{\rm offset} \\ & \qquad i = 2,3,4, \end{aligned} \quad (6)$$

where the coefficients a_i, b_i and c_i for the three generators are listed in the Appendix. From (3) to (6), the utility function, $U(k)$, depends only on the plant output vector, $y(k)$, and the control action vector, $u(k)$. As defined in (1), the cost-to-go function, $J(k)$, is then the discounted accumulation of $U(k)$. The approximation of $J(k)$ is accomplished by the critic network.

An RNN DHP critic network is trained online to approximate $\lambda(k+1)$, the derivative of $J(k+1)$ with respect to $y(k+1)$, by minimizing the following error [29]:

$$\begin{aligned} E_c(k) &= \|e_c(k)\|^2 \\ e_c(k) &= \hat{\lambda}(k) - \left\{\frac{\partial U(k)}{\partial y(k)} + \frac{\partial U(k)}{\partial u(k)}\frac{\partial u(k)}{\partial y(k)} \right. \\ &\quad \left. + \gamma\hat{\lambda}(k+1)\left[\frac{\partial \hat{y}(k+1)}{\partial y(k)} + \frac{\partial \hat{y}(k+1)}{\partial u(k)}\frac{\partial u(k)}{\partial y(k)}\right]\right\}. \end{aligned} \quad (7)$$

The training of the critic network is done online with the action network in loop. The training starts with a small discount factor γ, say 0.5. As the critic weights converge, the discount factor is linearly increased to 0.8 in this paper. A higher discount factor results in a higher number of look-forward steps but requires longer training. Since the training of the action network also depends on the critic network [29], these two networks are trained and converge together [35].

D. Action Network—Optimal Control Law Approximation

The optimal control objective of the DSOPF controller is to minimize $J(k)$ at every time step k, which is accomplished by training the action network. An RNN action network is trained to approximate the optimal control law by minimizing [29]

$$\begin{aligned} E_a(k) &= \left\|\frac{\partial \hat{J}(k)}{\partial u(k)}\right\|^2 \\ \frac{\partial \hat{J}(k)}{\partial u(k)} &= \frac{\partial U(k)}{\partial u(k)} + \gamma\hat{\lambda}(k+1)\frac{\partial \hat{y}(k+1)}{\partial u(k)}. \end{aligned} \quad (8)$$

During the training, when $E_a(k)$ becomes zero, $u(k)$ is the optimal control action that minimizes $J(k)$ in the local region. Global optimal is obtained by exposing the DSOPF controller to different system conditions.

To minimize the initial impact on the power system, the random initial weights of the critic and action networks are limited to very small values such that the initial outputs of both networks are close to zero [18], [41]. Starting at D1 (see Table I) and with a discount factor of 0.5, the action and critic networks are connected to the 12-bus system and trained online. The weights of both the action and critic networks are updated in every time step, i.e., 1 s, based on their error signals (see Fig. 3). Different disturbances are then applied the system. After both networks converge at D1, the training process continues at other operating points, and the discount factor is slowly increased.

V. Simulation Results

A. Steady-State Performance of DSOPF Control

The steady-state performance of the DSOPF controller is studied at multiple dispatch cases. Due to limited space, only the results at D1, D3, and D7 are shown in Table II, where the system is driven by either the AGC2 + $\rm V_4$Ctrl or the DSOPF controller. For $\rm V_4$Ctrl, the reference voltage at bus 4 is set to 0.97 pu. The voltages of the two load buses, V_4 and V_5, and the

TABLE II
STEADY-STATE COMPARISONS OF THE PROPOSED DSOPF CONTROL AND AGC2 + V_4 CTRL (FUEL: K$/H, f: HZ, P_{tie}: MW, P_{loss}: MW, V: PU, S: PU)

	D1			D3			D7	
	AGC2+ V_4Ctrl	DSOPF Ctrl		AGC2+ V_4Ctrl	DSOPF Ctrl		AGC2+ V_4Ctrl	DSOPF Ctrl
Utility	**7.90**	**7.21**	***Utility***	**9.74**	**8.81**	***Utility***	**10.75**	**10.12**
Fuel	43.67	43.24	*Fuel*	44.23	43.61	*Fuel*	46.18	45.98
F	60.000	60.001	f	60.000	60.003	f	60	60.003
P_{tie}	480.0	479.6	P_{tie}	480.0	478.9	P_{tie}	480	479.1
P_{loss}	46.3	40.5	P_{loss}	46.7	39.1	P_{loss}	48.7	41.9
U_{Volt}	**1.619**	**1.142**	U_{Volt}	**2.937**	**2.391**	U_{Volt}	**2.14**	**1.586**
V_4	0.970	0.976	V_4	0.970	0.967	V_4	0.970	0.973
V_5	0.993	1.007	V_5	0.979	1.003	V_5	0.984	1.007
U_{Line}	**1.904**	**1.813**	U_{Line}	**1.868**	**1.754**	U_{Line}	**1.900**	**1.793**
S_{25}	0.76	0.71	S_{25}	0.81	0.75	S_{25}	0.77	0.73
S_{16}	0.80	0.76	S_{16}	0.55	0.56	S_{16}	0.78	0.71
S_{78}	0.67	0.63	S_{78}	0.75	0.68	S_{78}	0.69	0.65
U_{Ctrl}	**0.244**	**0.602**	U_{Ctrl}	**0.244**	**0.668**	U_{Ctrl}	**0.028**	**0.337**

apparent power loading of the three most heavily loaded lines are listed in Table II.

By using the DSOPF control, the utility function, as an overall index of optimality, is lower at all three dispatch cases. Lower fuel cost, lower line loss, and lower peak line loading are achieved by the DSOPF control with higher control effort and slightly larger frequency and tie-line flow deviation.

B. DSOPF Control Performance After Load Tripping

The system is running at dispatch case D1. An unexpected contingency happens and causes the 100 MW 60 MVAr load at bus 5 to trip at 300 s. To prevent over-voltage, the capacitor bank at bus 5 is also tripped at 301 s. The system frequency and tie-line flow controlled by AGC2 + V_4Ctrl and the DSOPF controller are shown in Fig. 10(a). The DSOPF controller results in a smaller frequency rise and faster frequency recovery. The tie-line flow also has a smaller deviation and faster return to its scheduled value of 480 MW, when the DSOPF controller is used.

Fig. 10(b) shows the six controlled quantities, active power outputs, and terminal voltages of the three generators, during this event. To regulate the short-term power imbalance, AGC2 decreases generation from all three generators at their maximum ramp rates. In contrast, the DSOPF controller further utilizes the load-voltage characteristics and temporarily increases the generator voltages, which creates higher energy consumption at the local buses to balance the short-term over-generation.

C. DSOPF Control Performance With Large Varying Loads

In this case, 50 MW 10 MVAr of varying constant-power load, as shown in Fig. 11(a), are added to both buses 4 and 5. As a result, the system experiences large load ramping (both up and down) at a rate of 40 MW/min with a peak of 100 MW. This event is used to simulate the variability contribution from intermittent renewable generation resources.

With AGC2 and V_4Ctrl, the active power outputs and terminal voltages of the three generators varies up and down to follow the system load and regulate the bus 4 voltage, as shown in Fig. 11(g) and (h). Meanwhile, the system consumes more fuel, as shown in Fig. 11(b), and has higher line losses, as shown

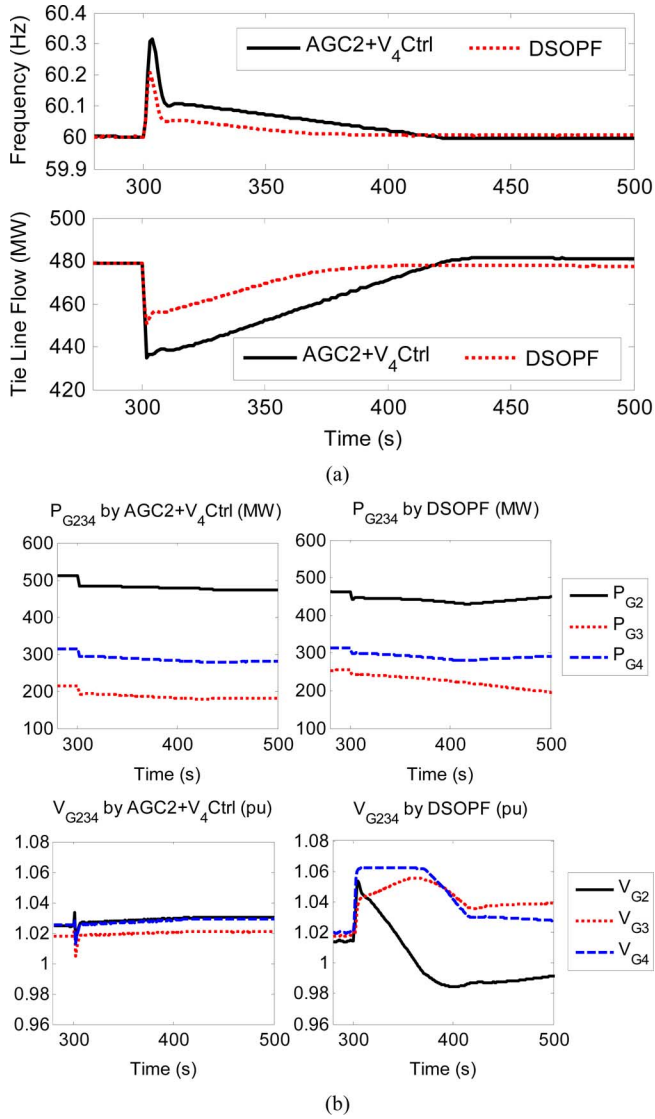

Fig. 10. System responses after load tripping at bus 5: (a) frequency and tie-line flow; (b) controlled variables.

in Fig. 11(c). The frequency and tie-line flow have a maximum deviation of more than 0.04 Hz and 15 MW, respectively, as shown in Fig. 11(d) and (e). Although the voltage at bus 4 is well regulated by V_4Ctrl, the voltage at bus 5 drops below 0.95 pu, as shown in Fig. 11(f). If this large load variation continues, frequent switching of the capacitor bank at bus 5 would be needed to avoid under-voltage violations.

On the contrary, with the DSOPF controller, the three generators are optimally coordinated. Lower fuel cost and line loss are achieved. The voltage at both buses 4 and 5 are now kept above 0.95 pu, while the system frequency and tie-line flow are regulated much closer to their nominal values.

D. DSOPF Control Performance After Line Outage

At dispatch case D7 (bus 4 becomes more heavily loaded), a three phase to ground fault happens somewhere along line 2–5 at 400 s. The fault is cleared by permanently tripping line 2–5. This is a severe event since line 2–5 is heavily loaded at D7 in order to serve the load at buses 4 and 5. Tripping of line 2–5 may cause overloading of the other two transmission corridors. This event requires a redistribution of power flow in order for the

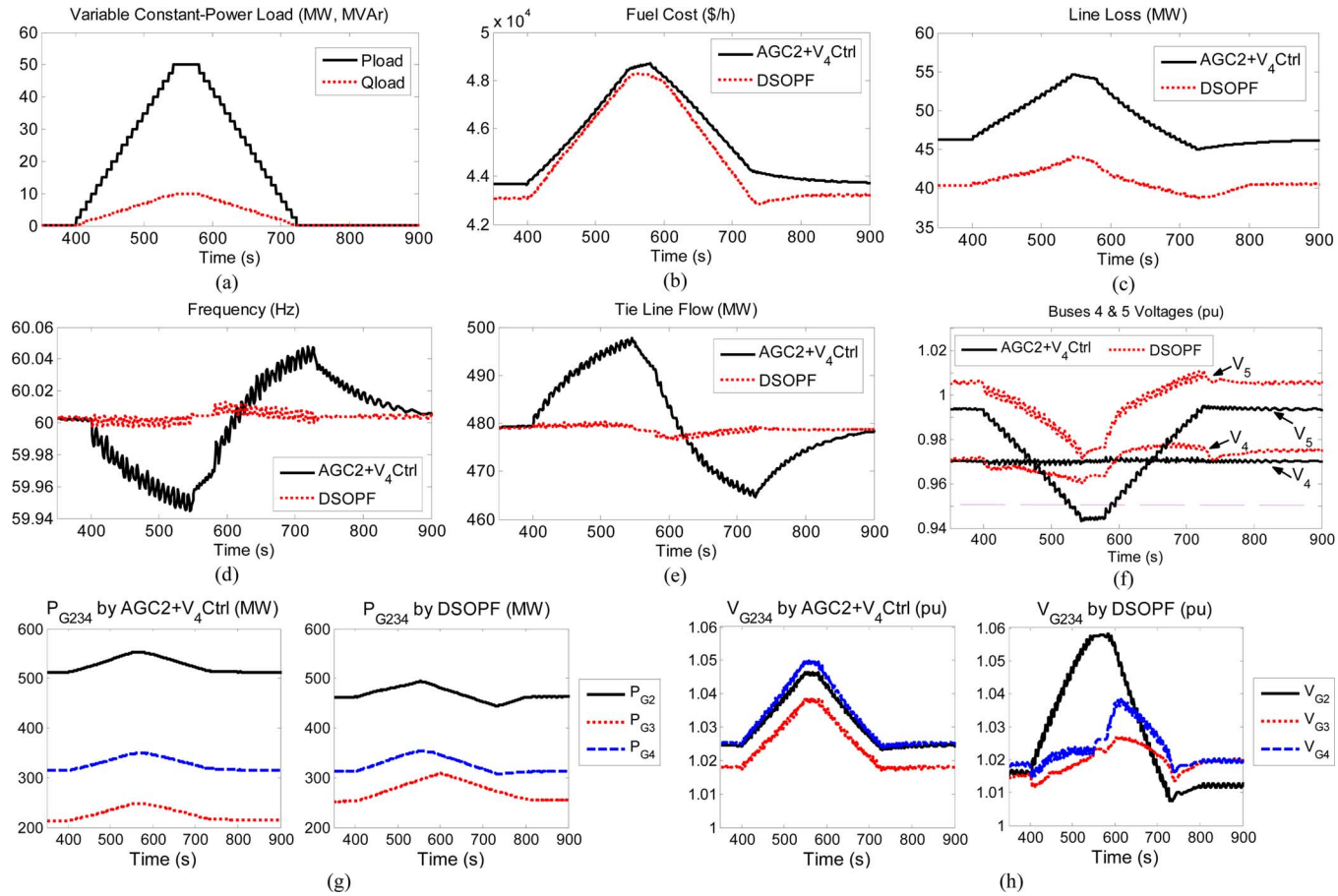

Fig. 11. System responses during large load variations at buses 4 and 5: (a) varying load applied to buses 4 and 5; (b)–(f): various system responses; (g)–(h): controlled variables.

12-bus system to survive. Fig. 12 shows the simulation results of this event with $\mathrm{AGC2} + \mathrm{V_4Ctrl}$ and the DSOPF controller.

When AGC2 and $\mathrm{V_4Ctrl}$ are used, bus 4 voltage (the lowest postfault voltage) drops below 0.94 pu, as shown in Fig. 12(a). The PI-based $\mathrm{V_4Ctrl}$ fails to regulate the bus 4 voltage, since the reactive support from G2 is interrupted and the reactive power outputs from G3 and G4 are limited by their MVA capacities. As a result, 50 MW 20 MVAr of load at bus 4 is tripped at 500 s to bring the bus 4 voltage back to normal condition. However, transmission line 1–6, which has the highest postfault line loading, remains overloaded, as shown in Fig. 12(b). Neither AGC2 nor $\mathrm{V_4Ctrl}$ is capable of relieving this line overload.

In contrast, with the proposed DSOPF controller, both the active and reactive power flows are optimally adjusted after the event. Both V_4 and S_{16} are maintained at normal conditions without violating any voltage or line limits. Under-voltage load shedding is thus not necessary. The system frequency, as shown in Fig. 12(c), also experiences less fluctuation. The system survives this event with the DSOPF controller.

VI. Practical Considerations

A. Data Selection and Pretraining

For practical development of the DSOPF controller, the pretraining of the model network can be executed offline using historical data obtained from the power system during its normal operation and disturbances. Using historical data allows the model network to learn the system dynamics during most operating conditions. Before connecting the DSOPF controller online for real-time control, the training of the action and critic networks can also be first conducted offline using high-accuracy nonlinear system models in real-time EMTP simulation tools. The ACD algorithm also shows promising capability to adapt to new operating conditions [18], [45], which allows the DSOPF controller to evolve and learn new optimal control rules.

B. Communication Delays

Power system wide-area communication delays range from several milliseconds to several seconds depending on the communication media and distance [46]. The performance of wide-area controllers may degrade if communication delays are not considered during the controller design stage. It has been shown that the neural network based modeling and control can successfully compensate for communication delays [18], [47], [48]. Further investigations are still needed on evaluating the effects of communication delays on the DSOPF controller and properly compensating for these delays during the design stage.

C. Scalability

Scalability is a major challenge for any power system control/optimization algorithms. For the DSOPF controller, novel neural network structures and training algorithms for large-scale neuroidentification and neurocontrol are two critical issues. Two concepts have been proposed by Venayagamoorthy—the concept of ObjectNets to provide modular solutions to neurocontrol of power systems [49], and the use of cellular neural networks

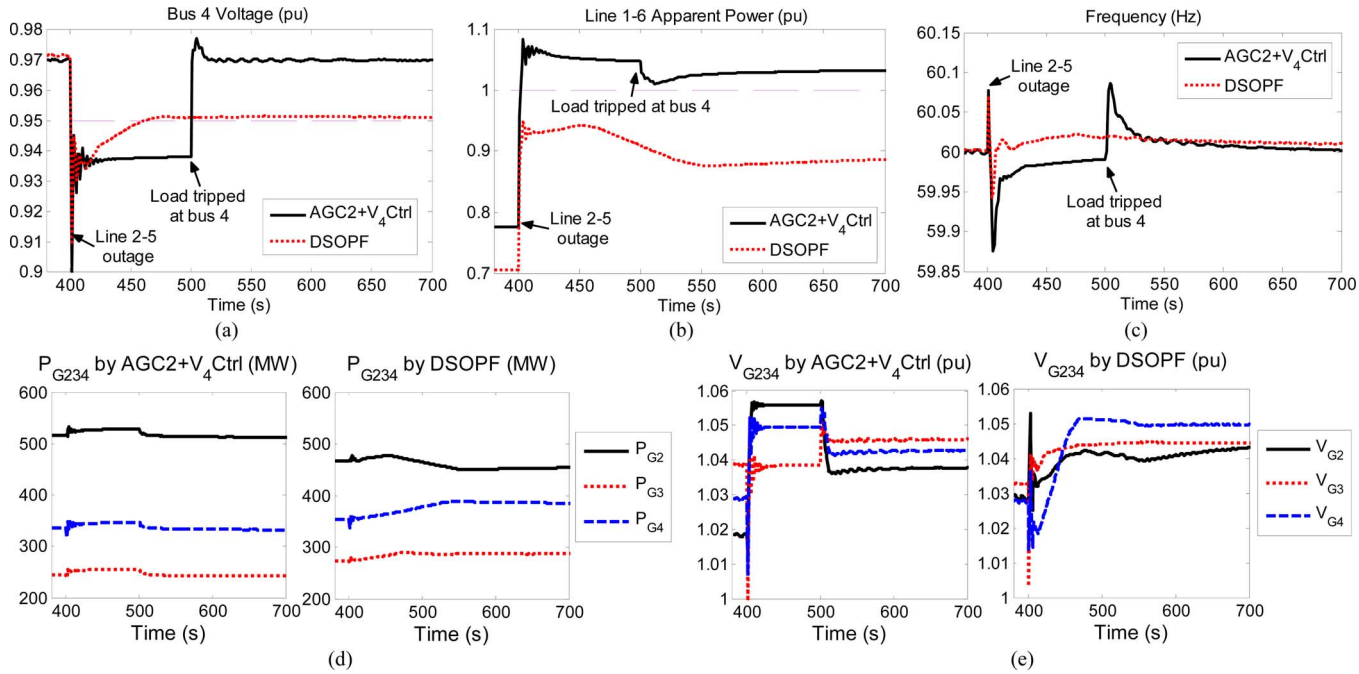

Fig. 12. System responses after line 2–5 outage (load tripping also occurs when AGC2 and V_4Ctrl are used): (a) system frequency; (b) bus 4 voltage; (c) line 1–6 loading; (d) active power outputs of G2 to G4; (e) terminal voltages of G2 to G4.

to capture topological dynamics of power systems [50]. Nevertheless, significant research efforts are still needed to investigate the scalability of the DSOPF control algorithm.

VII. Conclusion

A wide-area measurement based dynamic stochastic optimal power flow (DSOPF) control algorithm using the adaptive critic design (ACD) technique has been presented in this paper as a promising solution to the future smart grid operation in an environment with high short-term uncertainty and variability. The DSOPF control adapts the nonlinear optimal control technique from the ACD theory, replaces the traditional AGC and secondary voltage control, and provides closed-loop dynamic tracking of a power system's optimal operating point.

The dual heuristic dynamic programming-ACD approach using recurrent neural networks is used to design a DSOPF controller for a 12-bus test power system. Simulation results demonstrate promising steady-state and dynamic performances of the designed DSOPF controller under various operating conditions and system disturbances. In the 12-bus system example, only the generator active and reactive power is controlled. For a more complex power system, different FACTS devices at critical load buses and transmission lines can also be controlled by the DSOPF controller following the same design scheme to achieve a better and more efficient system-wide real-time optimal coordinated active and reactive power flow control. Scalability of the neurocontrol, which is still an on-going research, is a major challenge for applying the DSOPF control to a larger system. Modular, cellular and multilevel neurocontrol structures are key approaches to solve the scalability issue.

Appendix

Base case and generator fuel cost coefficients of the 12-bus power system (modified from [42]):

1) Generator Buses

Bus	Gen MVA	V_G* (pu)	P_G* (MW)	Fuel Cost ($/h) a	b	c
9 (G1)	1000	1.02	480			
10 (G2)	700	1.02	500	700	34.10	0.0117
11 (G3)	500	1.01	200	670	36.85	0.0135
12 (G4)	500	1.02	300	650	36.24	0.0130

Scheduled area power import P_{tie}* = 480 MW.

2) Load Buses

Bus	Load (MVA) Const. Impedance	Const. Power	Shunt Cap. (MVAr)
2	140 + j100	140 + j100	
3	160 + j120	160 + j120	
4	160 + j120	160 + j120	160
5	50 + j30	50 + j30	80
6	220 + j150	220 + j150	180

Weighting factors and constants used in the utility function:

w_{freq}	w_{tie}	w_{volt}	w_{line}	w_{fuel}	F^{offset}	w_{loss}	w_{Pg}	w_{Vg}
400	0.01	1600	1	0.001	4e4	0.01	1e-4	200

References

[1] D. Maggio, C. D'Annunzio, S. Huang, and C. Thompson, "Outstanding questions around increasing variable generation penetration in the ERCOT system," in *Proc. 2010 IEEE PES Gen. Meet.*, Minneapolis, MN, Jul. 25–29, 2010.

[2] D. Hawkins, K. Parks, and J. Blatchford, "Improved power system operations with high penetration of wind power: A dialog between academia and industry," in *Proc. 2010 IEEE PES Gen. Meet.*, Minneapolis, MN, Jul. 25–29, 2010.

[3] K. Porter and J. Rogers, "Status of centralized wind power forecasting in North America: May 2009–May 2010," NREL Subcontract Rep. NREL/SR-550-47853, Apr. 2010.

[4] A. J. Wood and B. F. Wollenberg, *Power Generation, Operation, and Control*, 2nd ed. New York: Wiley-Interscience, Jan. 1996.

[5] S. Fink, C. Mudd, K. Porter, and B. Morgenstern, "Wind energy curtailment case studies," NREL Subcontract Rep. NREL/SR-550-46716, Oct. 2009.

[6] K. M. Chandy, S. H. Low, U. Topcu, and H. Xu, "A simple optimal power flow model with energy storage," in *Proc. 49th IEEE Conf. Decision Control (CDC)*, Atlanta, GA, Dec. 15–17, 2010.

[7] J. Lavaei and S. H. Low, "Convexification of optimal power flow problem," in *Proc. 48th Annu. Allerton Conf. Commun., Control, Comput.*, Monticello, IL, Sep. 29–Oct. 1 2010.

[8] P. Kundur, *Power System Stability and Control*. New York: McGraw-Hill, 1994.

[9] J. De La Ree, V. Centeno, J. S. Thorp, and A. G. Phadke, "Synchronized phasor measurement applications in power systems," *IEEE Trans. Smart Grid*, vol. 1, no. 1, pp. 20–27, Jun. 2010.

[10] D. Karlsson, M. Hemmingsson, and S. Lindahl, "Wide area system monitoring and control—Terminology, phenomena, and solution implementation strategies," *IEEE Power Energy Mag.*, vol. 2, no. 5, pp. 68–76, Sept.–Oct. 2004.

[11] E. Farantatos, G. K. Stefopoulos, G. J. Cokkinides, and A. P. Meliopoulos, "PMU-based dynamic state estimation for electric power systems," in *Proc. 2009 PES Gen. Meet.*, Calgary, AB, Canada, Jul. 2009.

[12] R. Huang, E. Farantatos, G. J. Cokkinides, and A. P. Meliopoulos, "Substation based dynamic state estimator—Numerical experiment," in *Proc. 2010 IEEE PES T&D Conf. Expo.*, New Orleans, LA, Apr. 19–22, 2010.

[13] I. Kamwa, R. Grondin, and Y. Hébert, "Wide-Area measurement based stabilizing control of large power systems—A decentralized/hierarchical approach," *IEEE Trans. Power Syst.*, vol. 16, no. 1, pp. 136–153, Feb. 2001.

[14] B. Chaudhuri, R. Majumder, and B. C. Pal, "Wide-area measurement based stabilizing control of power system considering signal transmission delay," *IEEE Trans. Power Syst.*, vol. 19, no. 4, pp. 1971–1979, Nov. 2004.

[15] R. Majumder, B. Chaudhuri, and B. C. Pal, "A probabilistic approach to model-based adaptive control for damping of interarea oscillations," *IEEE Trans. Power Syst.*, vol. 20, no. 1, pp. 367–374, Feb. 2005.

[16] S. Ray and G. K. Venayagamoorthy, "Wide-area signal-based optimal neurocontroller for a UPFC," *IEEE Trans. Power Del.*, vol. 23, no. 3, pp. 1597–1605, Jul. 2008.

[17] S. Ray, G. K. Venayagamoorthy, B. Chaudhuri, and R. Majumder, "Comparison of adaptive critic-based and classical wide-area controllers for power systems," *IEEE Trans. Syst., Man, Cybern. B, Cybern.*, vol. 38, no. 4, pp. 1002–1007, Aug. 2008.

[18] S. Mohagheghi, G. K. Venayagamoorthy, and R. G. Harley, "Optimal wide area controller and state predictor for a power system," *IEEE Trans. Power Syst.*, vol. 22, no. 2, pp. 693–705, May 2007.

[19] H. Ni, G. T. Heydt, and L. Mili, "Power system stability agents using robust wide area control," *IEEE Trans. Power Syst.*, vol. 17, no. 4, pp. 1123–1131, Nov. 2002.

[20] F. Okou, L. A. Dessaint, and O. Akhrif, "Power systems stability enhancement using a wind-area signals based hierarchical controller," *IEEE Trans. Power Syst.*, vol. 20, no. 3, pp. 1465–1477, Aug. 2005.

[21] G. Yu, B. Zhang, H. Xie, and C. Wang, "Wide-area measurement-based nonlinear robust control of power system considering signals' delay and incompleteness," in *Proc. IEEE PES Gen. Meet.*, Tampa, FL, Jun. 24–28, 2007.

[22] S. Corsi, M. Pozzi, C. Sabelli, and A. Serrani, "The coordinated automatic voltage control of the Italian transmission grid—Part I: Reasons of the choice and overview of the consolidated hierarchical system," *IEEE Trans. Power Syst.*, vol. 19, no. 4, pp. 1723–1732, Nov. 2004.

[23] S. Corsi, M. Pozzi, M. Sforna, and G. Dell'Olio, "The coordinated automatic voltage control of the Italian transmission grid—Part II: Control apparatuses and field performance of the consolidated hierarchical system," *IEEE Trans. Power Syst.*, vol. 19, no. 4, pp. 1733–1741, Nov. 2004.

[24] H. Wang, H. Li, and H. Chen, "Coordinated secondary voltage control to eliminate voltage violations in power system contingencies," *IEEE Trans. Power Syst.*, vol. 18, no. 2, pp. 588–595, May 2003.

[25] J. Wen, Q. Wu, D. Turner, S. Cheng, and J. Fitch, "Optimal coordinated voltage control for power system voltage stability," *IEEE Trans. Power Syst.*, vol. 19, no. 2, pp. 1115–1122, May 2004.

[26] B. Fardanesh, "Future trends in power system control," *IEEE Comput. Appl. Power*, vol. 15, no. 3, pp. 24–31, Jul. 2002.

[27] P. Werbos, "New directions in ACDs: Keys to intelligent control and understanding the brain," in *Proc. Int. Joint Conf. Neural Netw. (IJCNN)*, Como, Italy, Jul. 24, 2000, vol. 3, pp. 61–66.

[28] D. Prokhorov and D. Wunsch, "Adaptive critic designs," *IEEE Trans. Neural Netw.*, vol. 8, no. 5, pp. 997–1007, Sep. 1997.

[29] J. Si, A. Barto, W. Powell, and D. Wunsch, *Hanbook of Learning and Approximate Dynamic Programming*. New York: Wiley-IEEE Press, 2004, ISBN-13: 978-0471660545.

[30] G. K. Venayagamoorthy, "CAREER: Scalable learning and adaptation with intelligent techniques and neural networks for reconfiguration and survivability of complex systems," NSF CAREER Award ECCS 0348221 June 2004, (submitted to NSF in Jul. 2003).

[31] J. Momoh, "Towards dynamic stochastic optimal power flow," in *Hanbook of Learning and Approximate Dynamic Programming*, J. Si, A. Barto, W. Powell, and D. Wunsch, Eds. New York: Wiley-IEEE Press, 2004.

[32] N. Jaleeli, L. VanSlyck, D. Ewart, L. Fink, and A. Hoffmann, "Understanding automatic generation control," *IEEE Trans. Power Syst.*, vol. 7, no. 3, pp. 1106–1122, Aug. 1992.

[33] T. Yu, B. Zhou, K. Chan, L. Chen, and B. Yang, "Stochastic optimal relaxed automatic generation control in non-Markov environment based on multi-step $Q(\lambda)$$ learning," *IEEE Trans. Power Syst.*, vol. 26, no. 3, pp. 1272–1282, Aug. 2011.

[34] S. Mohagheghi, G. K. Venayagamoorthy, and R. G. Harley, "Adaptive critic design based neuro-fuzzy controller for a static compensator in a multimachine power system," *IEEE Trans. Power Syst.*, vol. 21, no. 4, pp. 1744–1754, Nov. 2006.

[35] G. K. Venayagamoorthy, R. G. Harley, and D. Wunsch, "Implementation of adaptive critic-based neurocontrollers for turbogenerators in a multimachine power system," *IEEE Trans. Neural Netw.*, vol. 14, no. 5, pp. 1047–1064, Sep. 2003.

[36] D. Prokhorov, G. Puskorius, and L. Feldkamp, "Dynamical neural networks for control," in *A Field Guide to Dynamical Recurrent Networks*. New York: Wiley-IEEE Press, 2001.

[37] J. Liang, J. Dai, G. Venayagamoorthy, and R. Harley, "Dynamic system eigenvalue extraction using a linear echo state network for small-signal stability analysis—A novel application," in *Proc. IEEE Int. Joint Conf. Neural Netw. (IJCNN)*, Barcelona, Spain, Jul. 18–23, 2010.

[38] S. Haykin, *Neural Networks: A Comprehensive Foundation*, 2nd ed. Englewood Cliffs, NJ: Prentice-Hall, 1998.

[39] H. Jaeger, "Tutorial on Training Recurrent Neural Networks, Covering BPTT, RTRL, EKF and the 'Echo State Network' Approach," German National Research Center for Information Technology, GMD Rep. 159, 2002.

[40] K. Narendra, "Neural networks for control theory and practice," *Proc. IEEE*, vol. 84, no. 10, pp. 1385–1406, Oct. 1996.

[41] J. Liang, R. G. Harley, and G. K. Venayagamoorthy, "Adaptive critic design based dynamic optimal power flow controller for a smart grid," in *Proc. 2011 IEEE Symp. Series \Comput. Intell. (SSCI)—CIASG*, Paris, France, Apr. 11–15, 2011.

[42] S. Jiang, U. D. Annakkage, and A. M. Gole, "A platform for validation of FACTS models," *IEEE Trans. Power Del.*, vol. 21, no. 1, pp. 484–491, Jan. 2006.

[43] IEEE Task Force on Load Representation for Dynamic Performance, "Load representation for dynamic performance analysis," *IEEE Trans. Power Syst.*, vol. 8, no. 2, pp. 472–482, May 1993.

[44] R. Zimmerman, MATPOWER User's Manual May 2010 [Online]. Available: http://www.pserc.cornell.edu/matpower/manual.pdf

[45] J. W. Park, G. K. Venayagamoorthy, and R. G. Harley, "MLP/RBF neural-networks-based online global model identification of synchronous generator," *IEEE Trans. Ind. Electron.*, vol. 52, no. 6, pp. 1685–1695, Dec. 2005.

[46] K. E. Holbert, G. T. Heydt, and H. Ni, "Use of satellite technologies for power system measurements, command, and control," *Proc. IEEE*, vol. 93, no. 5, pp. 947–955, May 2005.

[47] W. Qiao, G. K. Venayagamoorthy, and R. G. Harley, "Optimal wide-area monitoring and nonlinear adaptive coordinating neurocontrol of a power system with wind power integration and multiple FACTS devices," *Neural Netw.*, vol. 21, no. 2–3, pp. 466–475, Mar.–Apr. 2008.

[48] S. Ray and G. K. Venayagamoorthy, "Real-time implementation of a measurement based adaptive wide area control system considering communication delays," *IET Proc. Gener., Transm., Distrib.*, vol. 2, no. 1, pp. 62–70, Jan. 2008.

[49] G. K. Venayagamoorthy, "Dynamic optimization of a multimachine power system with a FACTS device using identification and control ObjectNets," in *Proc. IEEE IAS Annu. Meet.*, Seattle, WA, Oct. 3–7, 2004.

[50] G. K. Venayagamoorthy, "Dynamic, stochastic, computational and scalable technologies for smart grid," *IEEE Comput. Intell. Mag. (Special Issue on Smart Grid)*, vol. 6, no. 3, pp. 22–35, Aug. 2011.

Jiaqi Liang (S'08) received the B.Eng. degree in electrical engineering from Tsinghua University, Beijing, China, in 2007, and the M.S. degree in electrical engineering from Georgia Institute of Technology, Atlanta, in 2009. He is currently working toward the Ph.D. degree in the Electric Energy Group, School of Electrical and Computer Engineering, Georgia Institute of Technology, Atlanta.

His research interests include electric machine control and their drive systems, power electronics, renewable energy grid integration, and power system control and operation.

Ganesh Kumar Venayagamoorthy (S'91–M'97–SM'02) received the Ph.D. degree in electrical engineering from the University of Natal, Durban, South Africa, in 2002.

He is the Duke Energy Distinguished Professor of Power Engineering, and a Professor of Electrical and Computer Engineering at Clemson University, Clemson, SC. Prior to that, he was a Professor of Electrical and Computer Engineering at the Missouri University of Science and Technology (Missouri S&T), Rolla, MO. He has published 2 edited books, 7 book chapters, and over 90 refereed journals papers and 290 refereed conference proceeding papers. His research interests are in the development and applications of advanced computational algorithms for power systems modeling, control and stability, smart grid applications, sensor networks, and signal processing.

Dr. Venayagamoorthy is a Fellow of the Institution of Engineering and Technology (IET), U.K., and the South African Institute of Electrical Engineers. He is a recipient of several awards including a 2007 U.S. Office of Naval Research Young Investigator Program Award, a 2004 NSF CAREER Award, the 2010 Innovation Award from St. Louis Academy of Science, the 2006 IEEE Power and Energy Society Outstanding Young Engineer Award, a 2011, 2008, 2007, and 2005 Missouri S&T Faculty Excellence Award, and a 2009 Missouri S&T Faculty Research Award. He has been involved in the leadership and organization of many conferences including the Founder and Chair of the 2011 IEEE Symposium of Computational Intelligence Applications in Smart Grid (CIASG). He is the Chair of the IEEE PES Working Group on Intelligent Control Systems (since 2005), the Chair of IEEE Computational Intelligence Society (CIS) Task Force on Smart Grid (since 2010), and the Chair of the IEEE PES Intelligent Systems Subcommittee (2011–2012). He is currently an Editor of the IEEE TRANSACTIONS ON SMART GRID and an Associate Editor of the IEEE TRANSACTIONS ON EVOLUTIONARY COMPUTATION.

Ronald G. Harley (M'77–SM'86–F'92) received the M.Sc.Eng. degree (*cum laude*) in electrical engineering from the University of Pretoria, Pretoria, South Africa, in 1965 and the Ph.D. degree from London University, London, U.K., in 1969.

He is currently a Regents' Professor with the School of Electrical and Computer Engineering, Georgia Institute of Technology, Atlanta, and also a Professor Emeritus with the University of KwaZulu-Natal, Durban, South Africa. He has coauthored more than 500 papers in refereed journals and international conference proceedings and holds 6 patents. His research interests include the dynamic behavior of electric machines, power systems and their components, and controlling them by the use of power electronics and intelligent control algorithms.

Dr. Harley is the recipient of the Cyril Veinott Electromechanical Energy Conversion Award in 2005 from the IEEE Power Engineering Society and the IEEE Richard Harold Kaufmann Technical Field Award in 2009.